JACS
JOURNAL OF THE AMERICAN CHEMICAL SOCIETY
Article
pubs.acs.org/JACS

Multiporphyrin Arrays with $\pi-\pi$ Interchromophore Interactions

Yuichi Terazono,[†] Gerdenis Kodis,[†] Mirianas Chachisvilis,[‡] Brian R. Cherry,[⊥] Maxime Fournier,[†] Ana Moore,*[,†] Thomas A. Moore,*[,†] and Devens Gust*[,†]

[†]Department of Chemistry and Biochemistry, Arizona State University, Tempe, Arizona 85287, United States
[‡]Solvexa, LLC, 3525 Del Mar Heights Road, #590, San Diego, California 92130-2122, United States
[⊥]Magnetic Resonance Research Center, Arizona State University, Tempe, Arizona 85287, United States

Supporting Information

ABSTRACT: A recently reported synthetic method has been employed to prepare several arrays of free base and zinc porphyrins. In the arrays, the porphyrins are arranged around a central benzene ring. The lack of aryl rings in the linkages to the central benzene ring, coupled with the presence of only one *meso*-aryl substituent on each porphyrin, allows strong electronic interactions between the porphyrin macrocycles. In arrays containing two or six porphyrins, a variety of evidence indicates that the porphyrins exist as twist-stacked dimers reminiscent of the special pairs of bacteriochlorophylls found in some photosynthetic bacteria. These dimers feature van der Waals contact between the macrocycles, and demonstrate excitonic splitting due to $\pi-\pi$ interactions. The excitonic effects split and blue-shift the Soret absorptions, and slightly broaden the Q-band absorptions and shift them to longer wavelengths. The interactions also lower the first oxidation potentials by ca. 100 mV, and the arrays show evidence for delocalization of the radical cation over both porphyrins in the dimer. The arrays demonstrate singlet−singlet energy transfer among the chromophores. Arrays of this type will be good models for some aspects of the interactions of photosynthetic pigments, including those of reaction center special pairs and possibly quantum coherence effects. They can also be useful in artificial photosynthetic constructs.

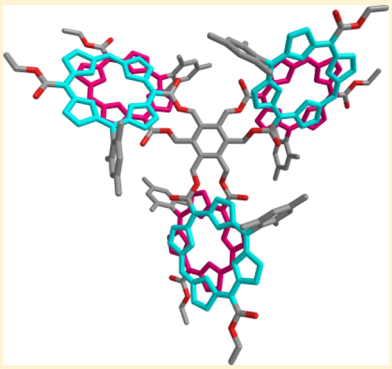

INTRODUCTION

Most of the sunlight used in photosynthesis is absorbed by light-gathering antenna molecules, rather than reaction centers where conversion to electrochemical potential occurs. Although antenna systems vary considerably from organism to organism,[1−4] a large fraction of antennas use chlorophylls as light absorbers. These chlorophylls are arranged in arrays featuring relatively strong interactions among the chromophores that permit very rapid and efficient singlet−singlet energy transfer between them. A variety of antenna architectures are known, including rings[5] of chlorophylls and carotenoids. Some reaction centers also feature multiple chlorophylls with strong electronic interactions.[6,7] Synthetic arrays in which porphyrins are arranged in ring-like structures have been prepared and studied in order to model the natural antennas and reaction centers and for potential use in artificial photosynthesis.[8−23] In some of these, the chromophores are held in large macrocyclic structures via covalent bonds[8,9,12] or self-assembly.[24] In others,[11,14,25] the porphyrins are organized in wheel-like structures whose covalent "spokes" are joined to a central hub. We and others have found hexaphenylbenzene to be an especially useful hub.[10,26−33] The various hexaphenylbenzene-based porphyrin arrays have shown interesting energy- and electron-transfer phenomena. However, the interactions between the porphyrins and other antenna chromophores linked to the hexaphenylbenzene core have not been as strong as those observed in some natural photosynthetic antennas[34−42] because the central hexaphenylbenzene hub limits close approach of the chromophores, and the porphyrins used have in general been tetra-arylporphyrins whose aryl groups inhibit close approach of the macrocyclic π-electron systems.

We recently reported a new synthetic method for the preparation of porphyrins that places a carboxylic acid group directly on one or more of the *meso*-carbon atoms, and produces porphyrins having only one *meso*-aryl substituent.[43] The acid moiety is available for further functionalization, and because there is no aryl group between it and the porphyrin ring, it allows construction of arrays in which the porphyrin macrocycles are closer together than in hexaphenylbenzenes and some related structures, and therefore can interact more strongly. Herein we describe the synthesis and the spectroscopic and electrochemical properties of several new cyclic porphyrin arrays constructed using this chemistry (Figure 1). The UV−vis and NMR spectroscopic data show that in these arrays the porphyrins associate intramolecularly via $\pi-\pi$ interactions, resulting in significant perturbations of steady-state and time-resolved spectral properties and electrochemical behavior and rapid singlet−singlet energy transfer among chromophores.

Received: October 6, 2014
Published: December 16, 2014

DOI: 10.1021/ja510267c
J. Am. Chem. Soc. 2015, 137, 245−258

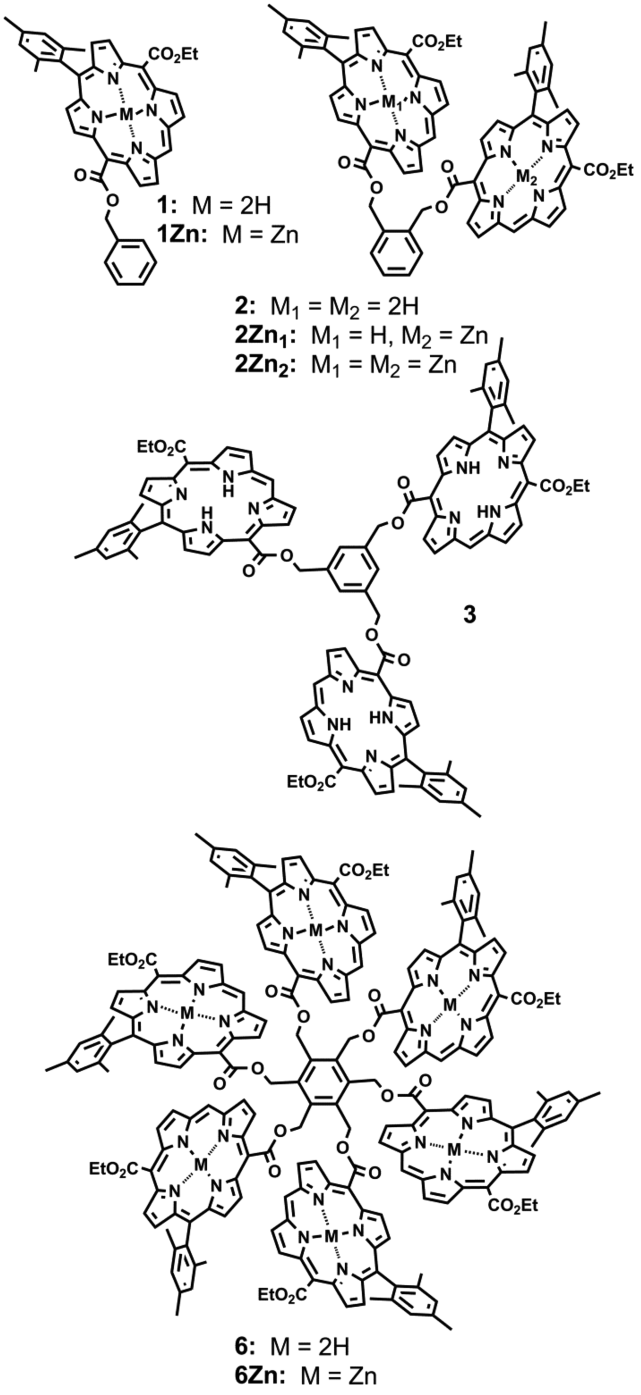

Figure 1. Structures of the porphyrin arrays.

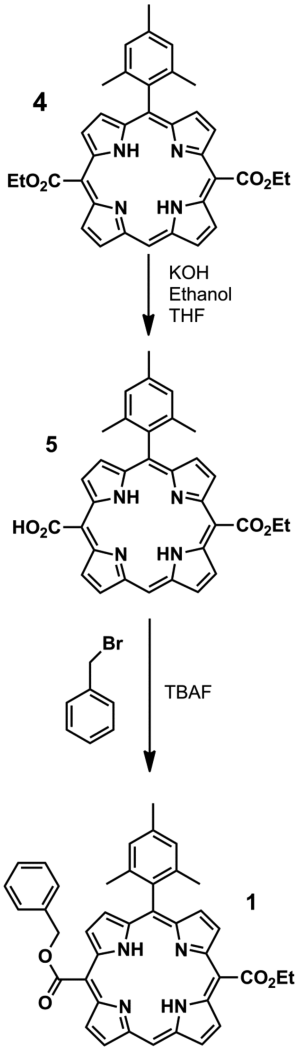

Figure 2. Synthetic scheme for preparation of **1**. The routes to **2**, **3**, and **6** were similar, but the benzyl bromide was replaced by the appropriate benzyl halide: THF = tetrahydrofuran, TBAF = tetra-*n*-butylammonium fluoride.

RESULTS

Synthesis. Given the availability of the *meso* carboxylic acid derivatives, preparation of the arrays was reasonably facile. The synthesis of **1** is shown in Figure 2, and similar chemistry was used to prepare the arrays. For **1**, porphyrin diester **4** was prepared as described earlier.[43] Controlled base-catalyzed hydrolysis yielded the monoester **5**. Coupling **5** to alcohols or amines using common coupling agents such as carbodiimides and dimethylaminopyridine was not successful. Evidently the intermediate *O*-acylisourea either does not form or is so stabilized by the porphyrin macrocycle that it is unreactive. However, we found that tetrabutylammonium fluoride (TBAF)-assisted esterification[44] by reaction of the acid with a benzyl bromide or chloride smoothly converted the acid to the corresponding ester. Reactions were performed in the presence of air and went smoothly to give the desired products in good yields. Even the hexad was obtained in about 80% yield, with almost no intermediates such as porphyrin triads, tetrads, or pentads. It is likely that the high yields and lack of intermediates are due to intermolecular porphyrin $\pi-\pi$ stacking interactions that bring reactants into close proximity. Such $\pi-\pi$ stacking effects were also postulated by Biemans et al. to explain a lack of intermediates in the synthesis of other porphyrin arrays.[45] To make the metalated analogues, zinc was introduced using zinc acetate dihydrate. Details of the syntheses and characterization of the compounds are given in the Supporting Information.

Conformations of the Arrays: Nuclear Magnetic Resonance and Theoretical Studies. There are four single bonds in the linkages joining a *meso* carbon atom of each porphyrin to the central benzene ring in the arrays. Some degree of rotational freedom is expected about each of these bonds, which, coupled with the presence of only one aryl ring per porphyrin, is expected to allow the porphyrin rings to approach one another and interact via attractive face-to-face

DOI: 10.1021/ja510267c
J. Am. Chem. Soc. 2015, 137, 245−258

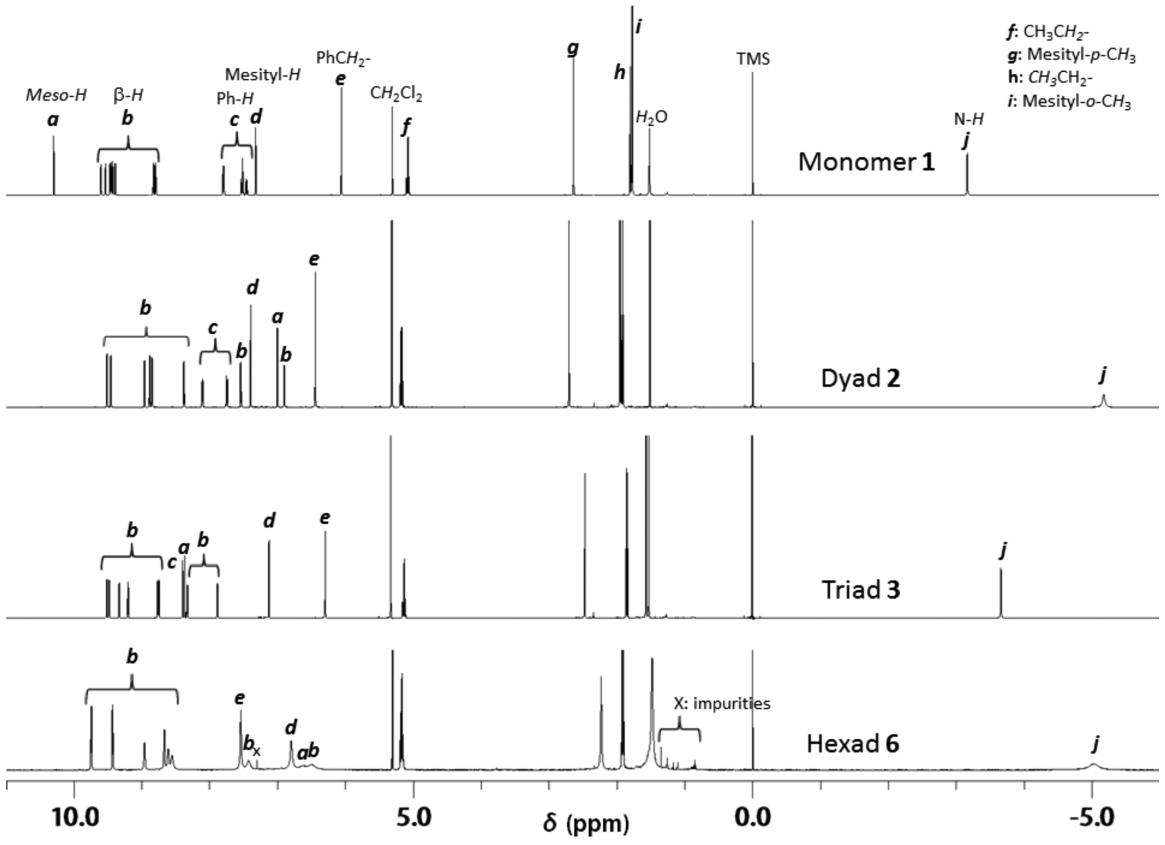

Figure 3. 400 MHz ^{1}H NMR spectra of the free base porphyrin arrays at 25 °C in deuterated dichloromethane containing tetramethylsilane as a reference.

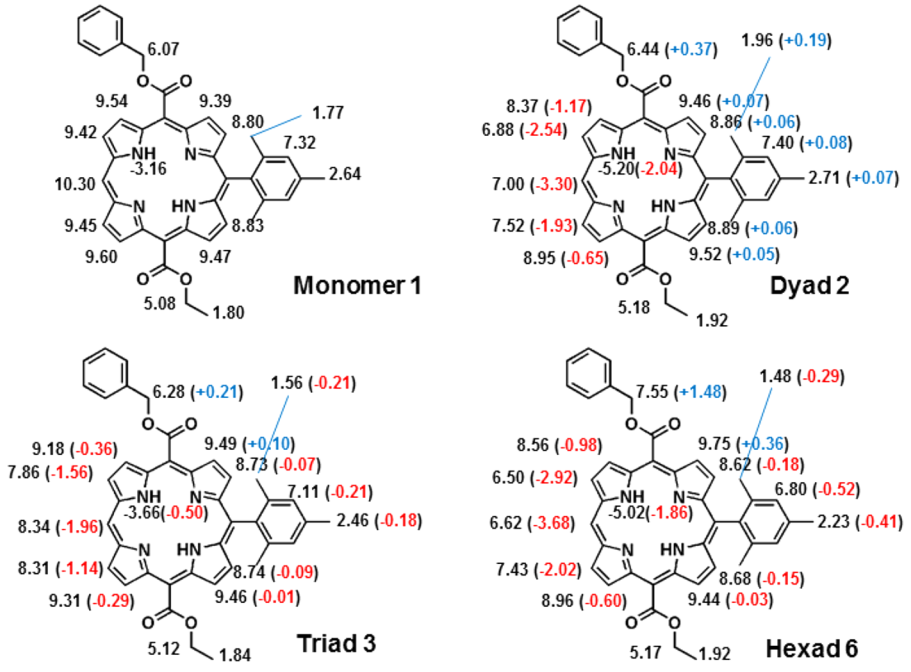

Figure 4. ^{1}H NMR chemical shifts (black), downfield chemical shift changes (blue), and upfield chemical shift changes (red) relative to compound **1** for **2**, **3**, and **6** based on the spectra shown in Figure 3. The additional substituents on the central benzene rings of the arrays are not shown.

$\pi-\pi$ interactions. Because porphyrins show strong shielding and deshielding ring current effects in NMR spectra, we investigated these spectra in order to detect any such interactions in the arrays, and obtain conformational information.

The ^{1}H NMR spectrum of monomer **1** in deuterated dichloromethane at 25 °C is shown at the top of Figure 3. Precursor porphyrin **5** and all of the porphyrins in the various linked compounds are ABCD porphyrins[46] in which all eight β-pyrrole protons are in constitutionally heterotopic environ-

DOI: 10.1021/ja510267c
J. Am. Chem. Soc. 2015, 137, 245−258

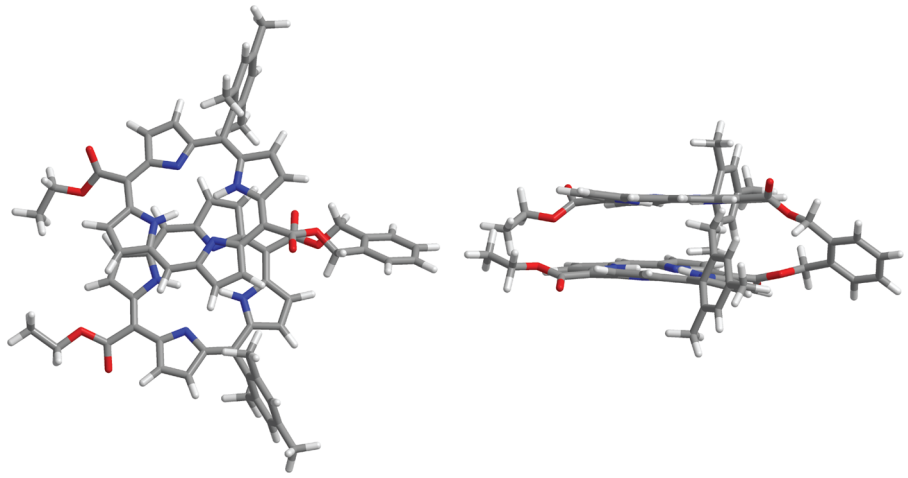

Figure 5. Top view (left) and side view (right) of the conformation of dyad **2** as determined by NMR spectroscopy.

ments. Thus, the spectrum of **1** features 8 resonances for these protons (labeled *b* in Figure 3). There is one *meso*-proton, and it appears as a single sharp resonance labeled *a*. The resonances for the *meso*- and *β*-protons appear relatively far downfield because they lie in the deshielding, peripheral region of the porphyrin ring current magnetic field.[47] The resonances for the N−H protons fall far upfield (resonance *j*), as these protons lie in the strongly shielded, central region of the macrocycle. There is only one resonance for these protons, as they rapidly chemically exchange on the NMR time scale at this temperature.

Turning now to dyad **2** (Figure 3), we first note that the same number of porphyrin resonances are present as were seen for **1**. This proves that either the structure of **2** has C_2 symmetry, with both porphyrins in identical environments, or else there is rapid averaging of the environments of the protons from the two individual rings on the NMR time scale. Second, it is apparent that there are large chemical shift changes for some of the resonances of **2** relative to **1**. These changes are summarized in Figure 4. The *meso*-proton resonance has moved upfield by 3.33 ppm, and the N−H proton by 2.04 ppm. Large *upfield* shifts are observed for four of the *β*-protons on one side of the macrocycle, while the four on the other side have moved *downfield* by very small amounts. Only very small changes have occurred for the protons of the mesityl group. Thus, the spectra are consistent with a conformation in which the two porphyrin rings are equivalent and stacked in a partial face-to-face arrangement in which the half of each porphyrin that does not bear a mesityl substituent lies above the corresponding region of the other porphyrin, with a separation of only a few Å.

We simulated the chemical shift changes for the protons of **2** using a molecular mechanics (MM2) generated structural model and the quantitative ring current model of Cross and Crossley,[47] and found a satisfactory fit of the experimental data for the conformation shown in Figure 5 (see Supporting Information Table S1). The C_2-symmetric structure shows that the porphyrins are in a twisted stack, with a ca. 3.5 Å separation of the macrocycle planes. This conformation suggests strong $\pi-\pi$ interactions between the macrocycles and is reminiscent of the arrangement of the two bacteriochlorophylls of the "special pair" of bacterial reaction centers.[7,48]

Because of the C_2 symmetry, the benzylic protons of **2** are diastereotopic, and should in principle have different chemical shifts. This is not observed. One possibility is that this is a case of accidental isochrony, where the two protons have chemical shifts that are apparently identical at this field strength. This may be the case, as the line width for these protons is approximately twice that for the resolved doublets. Alternatively, the environments of the two protons may be averaged by interconversion between enantiomers that is rapid on the NMR time scale. This might occur on the slow NMR time scale via rotations about the single bonds in the linkages between the porphyrin macrocycles and the central benzene ring, even though at any given time, essentially all of the molecules reside in one of the two enantiomeric forms.

A low-temperature study of the spectrum of **2** (Supporting InformationFigure S1) shows some additional shielding of some of the protons in the region where the macrocyclic rings are stacked on one another, but no splitting due to population of multiple conformers. The increased shielding may be due to slightly closer approach of the two macrocycles at lower temperatures, or a reduction in small-scale motions of the rings. The N−H protons split into two resonances at around 10 °C, and this is ascribed to the chemical exchange of these protons becoming slow on the NMR time scale.[49−52]

Selective NOE experiments on dyad **2** were also carried out. Irradiation of the *meso* proton of **2** at 7.00 ppm gave rise to a strong NOE in one of the *ortho* methyl groups of the *other* porphyrin at 1.96 ppm, corresponding to an internuclear distance of about 3 Å (Supporting Information Figure S12). A similar NOE was measured for the proton at 7.00 ppm when the methyl group at 1.96 was irradiated. Although these results alone do not permit calculation of a full solution structure, they confirm that the two porphyrins are in van der Waals contact essentially all the time.

Turning now to hexad **6**, Figures 3 and 4 show that the six porphyrins are again in equivalent environments, as indicated by the fact that no splitting of the resonances is observed. The *β*- and *meso*-protons on the half of the macrocyclic rings that lack mesityl groups are shielded by similar (although not identical) amounts to those observed for **2**. The same is true for the N−H protons (labeled *j*). These data suggest that **6** exists as a symmetric trimer of dimers, where each dimer has a conformation similar to that of **2**. However, there are additional shieldings observed for **6** that were not found in **2**. In particular, the mesityl aromatic and methyl group protons are shifted significantly upfield, as are the *β*-pyrrole protons closest to the mesityl group. These results indicate that the half of the

DOI: 10.1021/ja510267c
J. Am. Chem. Soc. 2015, 137, 245−258

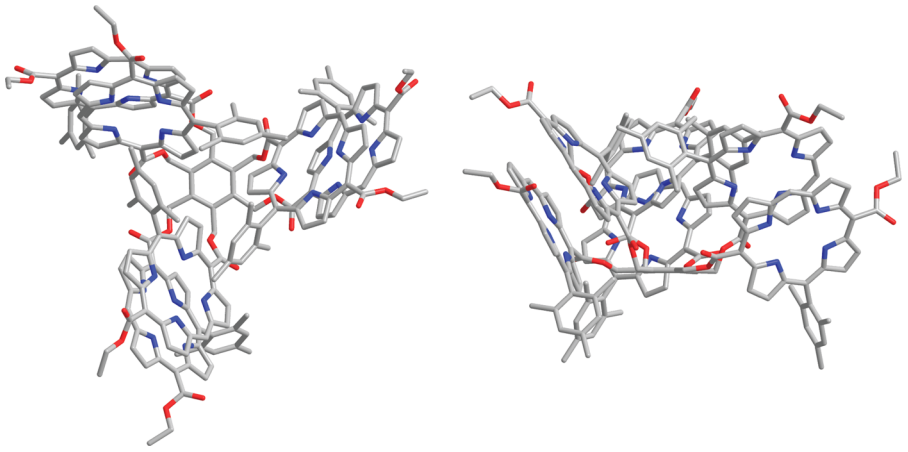

Figure 6. Top view (left) and side view (right) of hexad **6** as calculated by DFT methods. The hydrogen atoms are not shown. Note the C_3 symmetry and the trimer of dyads conformation.

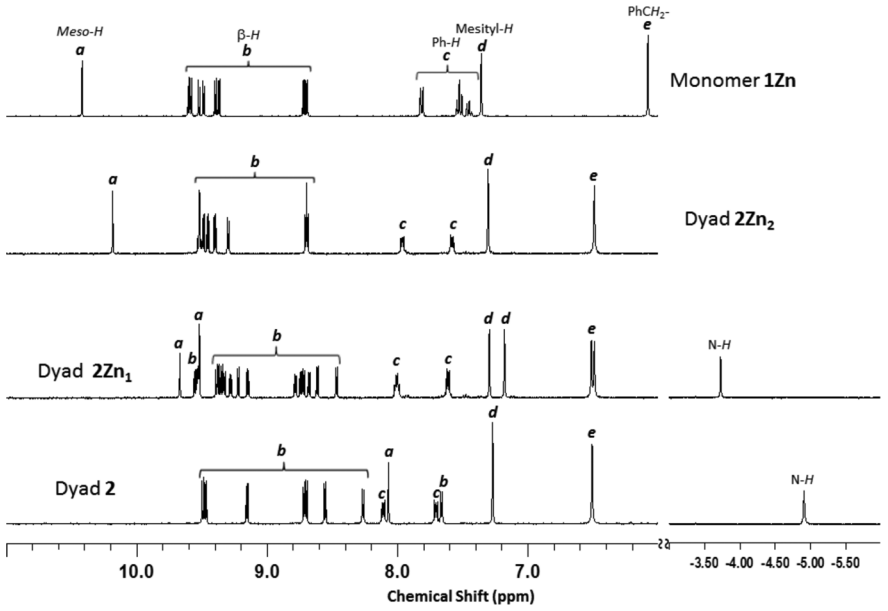

Figure 7. ^{1}H NMR spectra of **1Zn**, **2Zn$_2$**, **2Zn$_1$**, and free base dyad **2** at 25 °C in dimethyl sulfoxide-d_6.

macrocyclic rings bearing the mesityl group and the mesityl group itself are located in the shielding region of porphyrin macrocycles of adjacent dimers. That is, **6** exists in a conformation consisting of three identical twist-stacked dimers, each of which features ca. 3.5 Å separation of the porphyrin planes, and each of which interacts less strongly with adjacent dimers.

In order to obtain more information about the conformation of **6**, we undertook modeling of the structure using a dispersion-corrected density functional method (DFT-DCP).[53] The DFT-DCP method at the B3LYP/6-31+G(d,p) level has been successfully applied to modeling non-covalent interactions in chlorophyll dimers in photosynthetic structures.[54] Calculation on this large structure was very slow, and constraints on SCF had to be relaxed. After 3 months of continuous energy minimization, the structure shown in Figure 6 was obtained. This structure shows a trimer of dimers related by a C_3 symmetry axis, as expected from the NMR results. Each dimer has a structure very similar to that of **2** derived from NMR measurements. In addition, each dimer has part of one porphyrin ring in close proximity to the other dimers, in regions consistent with the shielding observed in the NMR spectra. In particular, one mesityl ring of each dimer is located in the strongly shielding region of a porphyrin ring of another dimer, and this is consistent with the mesityl shieldings observed in the NMR spectrum. In these respects, the calculated structure is consistent with the NMR results. However, the calculated structure features C_3 symmetry, rather than the D_3 symmetry seen in the NMR spectrum. All three dimers are located on the same side of the plane of the central benzene ring. One consequence of this is that each dimer in Figure 6 has not only a shielded mesityl group, as discussed above, but also a second mesityl ring in a region relatively far from the adjacent dimers.

The NMR and DFT results may be reconciled by postulating that the structure in Figure 6 is fluctuating on the NMR time scale between the one shown and an additional homomeric or enantiomeric structure in which the two macrocycles of each dimer have changed places, relative to the other dimers and the plane of the central benzene ring. Such a situation is consistent with the chemical shift changes between **2** and **6**, and with the fact that some of the *β*- and *meso*-resonances of **6** are

DOI: 10.1021/ja510267c
J. Am. Chem. Soc. 2015, 137, 245−258

broadened (Figure 3). This broadening is consistent with exchange of environments which is becoming slow on the NMR time scale. In order to investigate this phenomenon, we obtained the NMR spectrum of **6** in 1,1,2,2-tetrachloroethane-d_2 at 100 °C (Supporting Information Figure S2). At this temperature, all of the resonances of **6** sharpen to narrow lines, as expected for a fluxional process that has become rapid on the NMR time scale.

The NMR spectrum of triad **3** is also shown in Figure 3, and the chemical shift changes are indicated in Figure 4. As was the case for the other molecules, the number of resonances observed indicates that the three porphyrin moieties of **3** are in equivalent average environments. It will be noted that upfield shifts of the mesityl, *meso*-, and all but one of the β-protons relative to **1** occur. This suggests that the porphyrins of **3** tend to form twist-stacked dyads much like those found in **2** and **6**. However, the chemical shift changes are much smaller for **3** than they are for the other compounds. Two factors undoubtedly contribute to this fact. First, due to the *meta* relationship of the links of the three porphyrins to the central benzene ring, each porphyrin is constrained to be farther from its neighbors than in the other molecules. This likely limits the strength of the interporphyrin $\pi-\pi$ stacking interactions. Second, it may be that only two porphyrins at a time exhibit strong stacking, while the third is farther away. This would reduce the average shielding experienced by a porphyrin as the conformations of the molecule interconvert on the NMR time scale. This possibility is supported by the UV−vis spectral data (vide infra).

Turning now to the zinc-containing arrays, portions of the ^{1}H NMR spectra of **2**, **2Zn$_1$**, and **2Zn$_2$** are shown in Figure 7. The spectra were recorded in deuterated dimethyl sulfoxide, as the spectra of the zinc-containing porphyrins in $CDCl_3$ or CD_2Cl_2 were broad. The spectra show that dyad **2** still assumes a twist-stacked dyad conformation, as it does in CD_2Cl_2. Dyad **2Zn$_1$** shows some of the same shielding phenomena as **2**, but the chemical shift changes for the β-, *meso*-, and N−H resonances are not as large. For dyad **2Zn$_2$**, small upfield shifts are still apparent for some protons, but in general the spectra are not very different from those of **1Zn**. Thus, the spectra suggest that the porphyrins of **2Zn$_2$** form stacked dyads in which there may be less electronic interaction between the porphyrins than there is in **2**. Dyad **2Zn$_1$** shows more association between the macrocycles, but it is weaker than that in free base dyad **2**. Thus, the NMR results suggest that $\pi-\pi$ stacking attractive interactions are present, but reduced in both of the zinc dyads, relative to the free base. The NMR spectrum of **6Zn** (Supporting Information Figure S3) shows shielding of the β- and *meso*-protons that suggests that there are significantly larger $\pi-\pi$ stacking interactions among the porphyrins in this molecule as compared to the dyads.

UV−Visible Spectroscopic Properties. The UV−vis spectroscopic properties of the arrays are of major importance, since one purpose of the compounds is to investigate the effects of interchromophore interactions on these properties. In addition, the spectra can yield additional information concerning the conformations of the molecules. Figure 8 shows the UV−vis spectra of the free base series **1**, **2**, **3**, and **6** in dichloromethane at ambient temperatures. The spectra are shown with the extinction coefficients divided by the number of porphyrins in the array (e.g., $\varepsilon/2$ for **2**). Monomer **1** shows a Soret band at 408 nm and Q-band maxima at 506, 543, 583, and 638 nm. These bands are typical for porphyrins of this

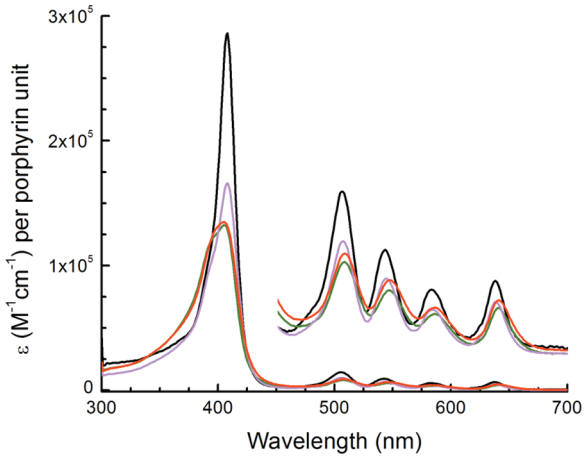

Figure 8. Absorption spectra in dichloromethane of **1** (black), **2** (green), **3** (magenta), and **6** (red). The inset is an offset 10-fold expansion of the *y*-axis scale. The extinction coefficient values given on the *y*-axis are the true extinction coefficients divided by the number of porphyrins in the array.

type; the Soret extinction coefficient of 2.8×10^5 M^{-1} cm^{-1} is between that of porphine (2.5×10^5 M^{-1} cm^{-1})[55] and typical *meso*-tetraarylporphyrins (ca. 4.0×10^5 M^{-1} cm^{-1}).[56] The spectrum of dyad **2** features the same transitions, but the spectra are perturbed. The Soret is blue-shifted, and has split into at least two overlapping peaks at 395 and 405 nm. This is characteristic of interchromophore excitonic interactions,[57,58] which are sometimes seen in stacked porphyrins or other chromophores.[58−65] The Q-bands appear at 508, 546, 586, and 640 nm. In addition to the ca. 3 nm shift to longer wavelengths, the Q-bands are broadened, relative to those of **1**, and the extinction coefficients at the maxima are reduced. Related effects have been reported for the spectra of intermolecularly associated porphyrin dimers.[62]

Figure 8 also shows the absorption spectrum of hexad **6** in dichloromethane. The absorption maxima and extinction coefficients are given in the Supporting Information (see synthesis and characterization). It is apparent that the spectrum of **6** closely resembles that of **2**. The Soret band is broadened and split in a similar fashion to that of **2**, and the Q-bands are also broadened and shifted to longer wavelengths. Thus, the spectrum of **6** is consistent with the trimer of dimers structure discussed above, with major excitonic interactions between porphyrins in pairs, and weaker interactions between different dimers. Triad **3**, on the other hand, features a sharper Soret band with a maximum at 408 nm, like monomer **1**, but the band is of reduced intensity and has a significant shoulder a few nm to the shorter wavelengths. The Q-bands also have maxima close to those of **1**, but are somewhat broadened relative to that compound. Thus, the UV−vis spectral data are consistent with the NMR data in showing that the effects of dimer formation in **3** are not as pronounced as they are in **2** and **6**. Given the *meta* arrangement of the linkages of the porphyrins of **3** to the central benzene ring, it is reasonable to expect that dimer formation would be different in **3** and the other compounds. One possibility is that at any one time, two of the porphyrins of **3** form a dimer structure, whereas the third exists in a non-associated form. The spectrum of the Soret region of **3** is consistent with this interpretation. It consists of a sharp peak near the wavelength maximum for monomer **1** superimposed on a broader feature similar to the Soret regions of **2** and **6**.

DOI: 10.1021/ja510267c
J. Am. Chem. Soc. 2015, 137, 245−258

The fluorescence emission spectra of **1**, **2**, **3**, and **6** in toluene solution are shown in Figure 9, along with the Q-band

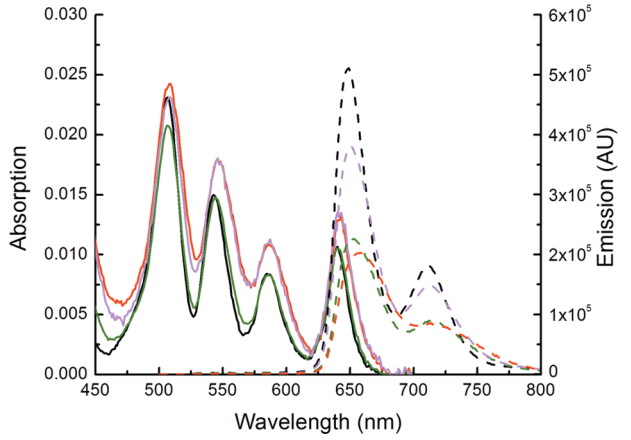

Figure 9. Absorption spectra (solid lines) and fluorescence emission spectra with excitation at 368 and/or 432 nm (dashes) in toluene solution of porphyrin **1** (black), dyad **2** (green), triad **3** (magenta), and hexad **6** (red). The emission spectra have been adjusted to reflect equal absorbance of all solutions at the excitation wavelength.

absorption spectra. The Soret absorption spectra (not shown) are similar to those in Figure 8 in that **1** and **3** show relatively sharp bands, whereas **2** and **6** show excitonic splitting. The Q-band absorption maxima are at essentially the same wavelengths as they are in dichloromethane. The emission of porphyrin **1** with excitation at 432 nm shows maxima at 649 and 711 nm. The spectrum of dyad **2** has maxima at 651 and 715 nm, triad **3** maxima are found at 650 and 713 nm, and the hexad **6** shows peaks at 658 and ca. 718 nm. Thus, the emission maxima of the arrays are shifted slightly to longer wavelengths relative to the model monomeric porphyrin. More importantly, the emissions of the arrays are broadened, relative to that of the monomer, the fluorescence quantum yield of **3** is somewhat reduced, relative to **1**, and the yields of **2** and **6** are about half that of the monomer (Table 1). Such a reduction of fluorescence quantum yield is characteristic of chromophores with excitonic interactions in which the higher-energy excitonic state is most allowed (see Discussion section).[57] In the present case, emission is from Q_x-band states, but these are populated by internal conversion from Soret excitation.

Turning now to the zinc-containing molecules, absorption spectra in toluene solution are shown in Figure 10a. Porphyrin

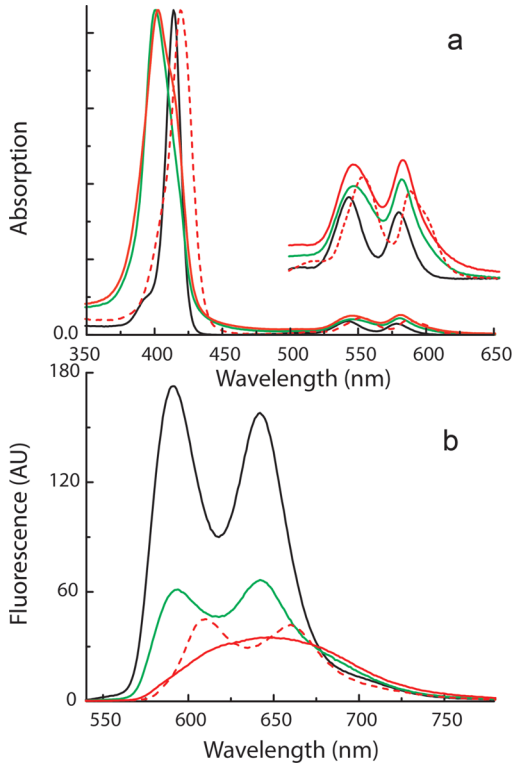

Figure 10. (a) Absorption and (b) fluorescence emission with excitation at 411 nm spectra in toluene solution of porphyrin **1Zn** (black), dyad **2Zn$_2$** (green), and hexad **6Zn** (red). The absorption spectra in (a) have been normalized at the Soret maxima. The emission spectra in (b) without addition of pyridine are from solutions with equal absorbance at the excitation wavelength. The dotted lines show spectra for a similar solution of hexad **6Zn** after the addition of a small amount of pyridine. The inset in (a) is times 6 along the *y* axis.

1Zn has maxima at 414 (Soret), 542, and 578 nm. The Soret maximum for dyad **2Zn$_2$** appears at 401 nm, and the hypsochromic shift relative to **1Zn** is accompanied by

Table 1. Fluorescence Quantum Yields and Decay Time Constants[a]

compd	λ_{em} (nm)	decay lifetime (% of decay)				χ^2	Φ_F[e]	anisotropy decay[d]	
1	650	4.03 ns (100)				1.04	0.07	114 ps	
	650	4.52 ns (100)[b]				1.02			
2	650	3.43 ns (88)	118 ps (12)			1.05	0.04	50 ps	210 ps
3	650	3.74 ns (70)	1.31 ns (13)	121 ps (17)		1.05	0.06		
6	650	3.73 ns (64)	937 ps (5)	70 ps (31)		1.01	0.04	50 ps	660 ps
	650	3.82 (59)[b]	882 ps (8)[b]	48 ps (34)[b]		1.10		35 ps[b]	480 ps[b]
1Zn	600	3.25 ns (100)				1.01	0.06	140 ps	
2Zn$_2$	600	2.84 ns (36)	1.51 ns (39)	67 ps (26)		1.01	0.03	50 ps	290 ps
2Zn$_1$	600/720[c]	3.62 nm	1.82 ns	700 ps	44 ps	1.02			
	600	3.07 ns (9)	1.51 ns (10)	42 ps (81)		1.01			
6Zn	600	1.97 ns (34)	864 ps (27)	89 ps (39)		1.01	0.02	40 ps	860 ps

[a]Measured in toluene with 400 nm excitation unless otherwise noted. [b]Measured in 2-methyltetrahydrofuran with 590 nm excitation. [c]Global fit over these wavelengths. [d]Measured in toluene at 660 nm with 590 nm excitation unless otherwise noted. [e]Measured in toluene; *meso*-tetraphenylporphyrin in toluene was used as fluorescence standard (ϕ_F = 0.11, from Murov, S. L.; Carmichael, I.; Hug, G. L. *Handbook of Photochemistry*, 2nd ed.; CRC: New York, 1993).

DOI: 10.1021/ja510267c
J. Am. Chem. Soc. 2015, 137, 245−258

significant broadening. The Q-bands appear at 546 and 580 nm, representing a bathochromic shift of these bands. The spectrum of **6Zn** is similar to that of **2Zn$_2$**, except that the Soret band shows even more broadening. Addition of a small amount of pyridine to the solution of **6Zn** results in considerable sharpening of the Soret absorption, and a bathochromic shift to slightly longer wavelengths than **1Zn**. Some sharpening is seen for the Q-bands upon addition of pyridine, and a bathochromic shift is also present. The red shifts are a well-known characteristic of coordination of pyridine to the zinc atoms of porphyrins, and coordination could interfere with porphyrin $\pi-\pi$ interactions.

The emission spectra of the zinc porphyrins in toluene solution are shown in Figure 10b. Porphyrin **1Zn** features sharp emissions at 591 and 642 nm that have an approximate mirror image relationship to the Q-bands in absorption, which is typical. In dyad **2Zn$_2$**, the two maxima appear at 594 and 642 nm. Hexad **6Zn**, on the other hand, features a single broad emission band at 647 nm. The emission quantum yields for the dyad and hexad are reduced, relative to that of the monomer **1Zn**. In **6Zn**, the spectrum is featureless, which indicates an additional interchromophore interaction not present in the dyad. Addition of a small amount of pyridine partially disrupts the internal aggregation, and the emission again has two maxima, at 610 and 660 nm.

Time-Resolved Emission Studies. We investigated the fluorescence properties of the arrays as a function of time after excitation in order to determine the effects of interchromophore interactions on excited state lifetimes. In addition, the time scale of fluorescence is much shorter than that of NMR, and thus allows observation of the properties of individual conformations that may be rapidly interconverting on the NMR time scale. The single photon timing technique was employed with excitation at either 400 or 590 nm. Results are shown in Table 1.

Free Base Porphyrin Arrays. The emission of porphyrin **1** in toluene solution at 650 nm decays as a single exponential with a time constant of 4.03 ns. This lifetime is approximately half that typically found for free base porphyrins. Shortened lifetimes have been observed in other *meso*-substituted porphyrins, including "push-pull" porphyrins,[66−68] and may be due to charge-transfer character of the first excited singlet state resulting from the *meso* ester group. Dyad **2** under the same conditions shows lifetimes of 3.43 ns (88% of the decay) and 118 ps (12%). The two lifetimes suggest that the molecule exists in a major and a minor conformation (or possibly more closely related conformations whose lifetimes were not distinguished at the signal-to-noise ratio obtained). The excited state lifetimes of dyad **2** are both shorter than that of the monomer **1**, signaling electronic interaction between the chromophores in both conformations.

For triad **3**, Table 1 shows three exponential components of the decay, all with somewhat shorter lifetimes than that of monomer **1**. The lifetimes and percentages of these components are roughly consistent with the steady-state emission seen in Figure 9.

Hexad **6** in toluene shows a longest lifetime of 3.73 ns (64%) a short lifetime of 70 ps (31%), and a very small amount (5%) of a component with a lifetime of 937 ps.

Looking at the results for **1**, **2**, **3**, and **6**, it is apparent that **2**, **3**, and **6** all have multiple conformations that do not interconvert on the nanosecond time scale, and that most or all of these conformations feature interchromophore interactions that reduce the fluorescence lifetimes of the chromophores, relative to non-interacting species. Molecules **2** and **6** show relatively more perturbation than does **3**, which is consistent with the higher degree of twist-stacked dimer formation suggested by the NMR and steady-state UV−vis spectra.

Zinc Porphyrin Arrays. Turning now to the zinc series of arrays, the **1Zn** first excited singlet state decays with a time constant of 3.25 ns as a single exponential (Table 1). The dyad **2Zn$_2$** decay was fitted with three exponential processes with lifetimes of 2.84 ns (36%), 1.51 ns (39%), and 67 ps (26%). Thus, as with **2**, this molecule exists in several conformations, and the excited-state lifetimes are all shorter than that of the monomer **1Zn** due to interchromophore interactions. Hexad **6Zn** features three decay components, all of which are significantly shorter than the lifetime of **1Zn** (1.97 ns, 864 ps, and 89 ps). Thus, the molecule also resides in several conformations, all of which show strong interchromophore interactions.

Singlet−Singlet Energy Transfer. The strong interporphyrin interactions observed in the NMR and UV−visible spectroscopic results for the arrays suggest that singlet−singlet energy transfer between the porphyrins is likely. This does in fact occur, as illustrated by results for **2Zn$_1$**, a dyad that features one free base porphyrin and one zinc porphyrin. Figure 11a shows the absorption spectrum of **2Zn$_1$** in toluene. It is similar to a superposition of the spectra of **2** and **2Zn$_2$**, with a broadened Soret band indicating interchromophore inter-

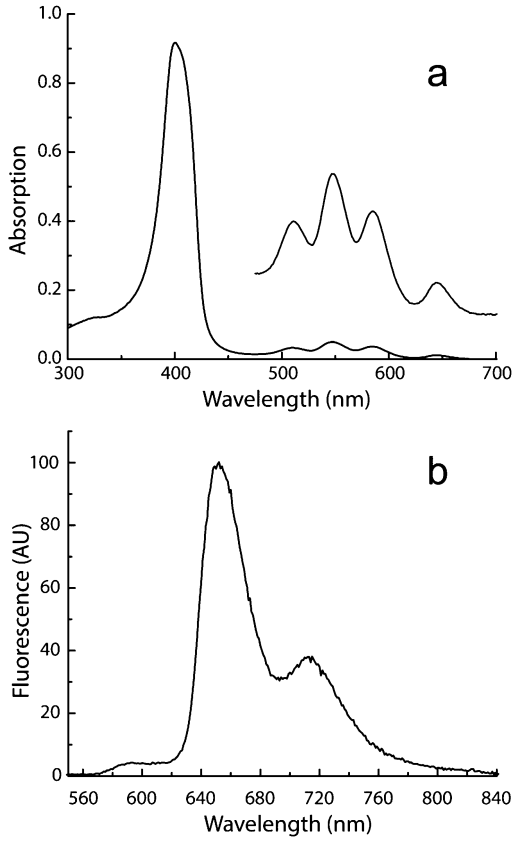

Figure 11. (a) Absorption and (b) fluorescence emission with excitation at 330 nm of the mixed dyad **2Zn$_1$** in toluene. The lack of emission from the zinc porphyrin moiety indicates highly efficient singlet−singlet energy transfer to the free base porphyrin.

DOI: 10.1021/ja510267c
J. Am. Chem. Soc. 2015, 137, 245−258

actions similar to those of the other dyads. Figure 11b shows the fluorescence spectrum of $\mathbf{2Zn_1}$ in toluene with excitation at 330 nm, where the absorption by the zinc and free base chromophores is comparable. It is clear that even though the zinc porphyrin is being excited, emission is from the free base porphyrin, with only a trace of emission around 600 nm where the zinc porphyrin emits strongly. This result indicates that singlet−singlet energy transfer from the zinc porphyrin to the free base is essentially quantitative.

The time-resolved fluorescence data for $\mathbf{2Zn_1}$ in Table 1 shows that a global fit to data obtained at 600 and 720 nm yields time constants of 3.62 ns, 1.82 ns, 700 ps, and 44 ps. Note from Figures 9 and 10 that emission at 600 nm is almost entirely from the zinc porphyrin, and emission at 720 nm is mainly from the free base porphyrin. When the data at 600 nm are fitted alone, almost all the emission (81%) has a time constant of 44 ps. This is ascribed to decay of the zinc porphyrin excited singlet state by energy transfer to the free base. The rate constant for this energy transfer process is ca. 2.3×10^{10} s^{-1}.

Energy transfer in the other arrays is more difficult to investigate because all the porphyrins are identical. However, information may be derived from fluorescence anisotropy decay measurements. In these experiments, the decay of the fluorescence anisotropy occurs either by molecular motions that reorient the chromophores or by energy transfer. Anisotropy measurements on **1** with excitation at 590 nm and detection at 660 nm gave a single exponential decay of the anisotropy with a time constant of 114 ps (Supporting Information Figure S4). This is ascribed to tumbling of the molecule in solution, as energy transfer is not possible in this case. Similar measurements on free base hexad **6** yielded two decay components of 50 and 660 ps (Supporting Information Figure S5). The long component is assigned to overall reorientation of the molecule, and is longer than was observed for **1** because of the increase in molecular size. The short component could be due to porphyrin−porphyrin energy transfer to adjacent porphyrins or dimers, giving a time constant for energy transfer of ca. 150 ps. (Assuming that the transition dipoles of the hexad are randomized, the energy hopping time is 3 times longer than the depolarization time).[30] Alternatively, the 50 ps time constant could be due to internal motions of the chromophores about the single bonds in their linkages, or to a combination of the two processes.

In order to obtain more information on the situation, anisotropy measurements were made on **6** in a less-viscous solvent, 2-methyltetrahydrofuran. As seen in Supporting Information Figure S6 and Table 1, anisotropy decays of 35 and 480 ps were obtained. The 480 ps component is assigned to more rapid overall tumbling of the molecule in the less viscous solvent. The short component also decreases, suggesting that internal motions of the moieties may be responsible, at least in part, for the short component. These internal motions would consist of rotations about the single bonds in the linkages joining the porphyrins to the central benzene ring. Thus, either the time constants for energy transfer and internal motions may be very similar, such that the two processes cannot be distinguished by the anisotropy measurements, or energy transfer occurs on a time scale that is too short to observe in the anisotropy measurements. Given the time constant of 44 ps found for energy transfer in $\mathbf{2Zn_1}$, it seems likely that energy transfers among identical porphyrins in **6** would be slower than this, in light of the less favorable energetics for Förster transfer.[69,70] Thus, although we cannot entirely rule out ultrafast energy transfer on a time scale too short to observe in our measurement, it is likely that interchromophore singlet−singlet energy transfer in **6** occurs with time constants on the order of 150 ps. Similar experiments were carried out with the zinc series of arrays. As seen in Table 1, monomer **1Zn** displayed an anisotropy decay time of 140 ps. The decay of hexad **6Zn** showed two components, of 40 and 860 ps. Thus, the zinc series behaves in a similar fashion to the free base compounds.

Anisotropy experiments on the dyads gave consistent results. For free base dyad **2**, anisotropy decays of 50 and 210 ps were observed in toluene. The 210 ps time constant is due to overall tumbling of the dyad, and the 50 ps time is ascribed to internal motions and/or energy transfer. As seen in Table 1, very similar results were obtained for the zinc dyad.

Electrochemistry. Redox potentials for the arrays and monomers **1** and **1Zn** were measured by cyclic voltammetry in dichloromethane containing 0.1 M tetra-*n*-butylammonium hexafluorophosphate. The potentials were determined using internal ferrocene/ferrocenium and converted to SCE using a conversion factor of 0.46 V.[71] The results are given in Table 2.

Table 2. Redox Potentials from Cyclic Voltammetry

	V vs SCE			
compd	Ox_2	Ox_1	Red_1	Red_2
1	1.54[b]	1.28[b]	−0.90	−1.22
2	1.44[a]	1.19[b]	−0.89	−1.21
3	1.55[a]	1.27[b]	−0.85	−1.22[b]
6	1.46[a]	1.18[b]	−0.86	−1.25[b]
1Zn	1.36	1.04[b]	−1.08	
$\mathbf{2Zn_2}$	1.15	0.99[b]	−1.09	
6Zn	1.01	0.92	−0.82	−1.16
$\mathbf{H_2TPP}$[c]		1.02	−1.20	
ZnTPP[d]		0.78	−1.39	

[a]These are anodic peak potentials, as the waves were not reversible. [b]Quasireversible. [c]$E_{1/2}$ from Kadish, K.; Morrison, M. *J. Am. Chem. Soc.* **1976**, *98*, 3326−3328. [d]$E_{1/2}$ from D'Souza, F.; Zandler, M.; Tagliatesta, P.; Ou, Z.; Shao, J.; Van Caemelbecke, E.; Kadish, K. *Inorg. Chem.* **1998**, *96*, 877−910.

Porphyrin **1** is more difficult to oxidize and more easily reduced than H_2TPP. This is ascribed to the electron withdrawing effects of the ester groups directly attached to the *meso* positions of the macrocycle. The potentials for triad **3** are almost identical to those for **1**, suggesting that interactions among the chromophores are not strong enough to affect redox properties. The first oxidation potentials of dyad **2** and hexad **6** are about 100 mV lower than that of **1**. These changes indicate that in these molecules, the interactions among porphyrins are strong enough to affect the electrochemistry.

The cyclic voltammogram of **1** is shown in Figure 12a. The two reduction waves and the quasireversible oxidation with an anodic peak at 1.33 V vs SCE are each ascribed to one-electron processes. The second oxidation wave has an anodic peak at 1.60 V. Figure 12b shows the corresponding experiment for dyad **2** at the same concentration. The reduction waves look similar to those observed for **1**, albeit approximately twice the amplitude, and are ascribed to two-electron reductions; i.e., one electron for each porphyrin in the dyad. The first anodic oxidation peak, however, at 1.22 V, occurs at a potential about 100 mV lower than that for **1**, as mentioned above, and

DOI: 10.1021/ja510267c
J. Am. Chem. Soc. 2015, 137, 245−258

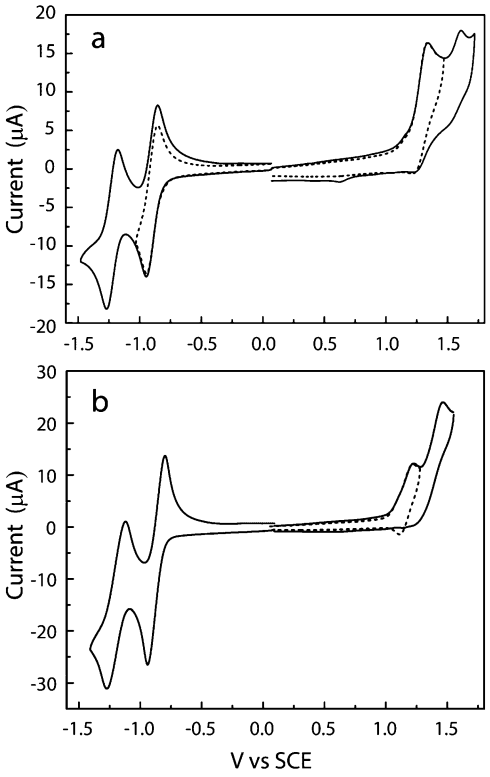

Figure 12. Cyclic voltammograms in dichloromethane solution containing 0.1 M tetra-*n*-butylammonium hexafluorophosphate of (a) monomer **1** and (b) dyad **2** under the same conditions.

interestingly, its amplitude corresponds to one electron per dyad molecule, rather than two. The second oxidation anodic peak is found at 1.44 V. The CV of triad **3** (Supporting Information Figure S7) features two reduction and one oxidation wave at potentials similar to those found for **1**, and the amplitudes are consistent with approximately three electrons per molecule. The CV for hexad **6**, on the other hand (Supporting Information Figure S8), shows a reduced amplitude for the first oxidation wave.

We propose that the reduced amplitudes for the first oxidations of **2** and **6** are due to delocalization of the radical cation over two (or possibly more in the case of **6**) porphyrin moieties with strong $\pi-\pi$ interactions. That is, the two porphyrins of, for example, **2** interact electronically due to the $\pi-\pi$ stacking. When one of the two porphyrins is oxidized, the resulting "hole" is shared by both porphyrins in the dimer. As a result, removal of the first electron occurs at a lower potential than it does for the monomer, and removal of a second electron occurs at a significantly higher potential than the first. This phenomenon is not observed for the reductions of **2**. Delocalization of a radical cation over two cyclic tetrapyrroles is characteristic of the strongly associated "special pair" of bacteriochlorophylls in some bacterial reaction centers.[72]

The cyclic voltammograms for monomer **1Zn** and dyad **2Zn$_2$** are shown in Supporting Information Figures S9 and S10, respectively. The voltammogram for **1Zn** shows first and second oxidation waves for the single porphyrin at 1.04 and 1.36 V vs SCE, respectively (Table 2). Dyad **2Zn$_2$** has a first oxidation at 0.99 V, which is slightly lower than that for **1Zn**. However, a second, overlapping wave is seen at 1.15 V. We assign these two waves to the first (0.99 V) and second (1.15 V) one-electron oxidations of the two porphyrin moieties of the dyad. Thus, as with **2**, removing a second electron from the molecule is significantly more difficult than removing the first. This is consistent with delocalization of the radical cation of **2Zn$_2$** over both porphyrins, as was discussed above for dyad **2**.

The cyclic voltammogram for hexad **6Zn** (Supporting Information Figure S11) shows a first oxidation at ~0.93 V vs SCE and additional, overlapping waves at higher potentials. The oxidations are irreversible under the conditions employed. The potential for the first oxidation is about 100 mV lower than that observed for **1Zn**, and indicates that the porphyrin moieties interact electronically, as has been observed for **6** and the dyads.

DISCUSSION

All of the spectroscopic and electrochemical data and molecular modeling results for the arrays are consistent with the presence of attractive $\pi-\pi$ interactions between adjacent porphyrins on the central benzene ring to form sets of partially stacked, dimeric structures. For dyad **2**, the NMR spectra show C_2 symmetry and strong shielding of roughly half of each macrocycle (the half that does not bear a mesityl ring). This shielding is due to the porphyrin aromatic ring current, and is consistent with the twist-stacked conformation shown in Figure 5, where the planes of the porphyrin macrocycles are at approximate van der Waals contact (ca. 3.5 Å). The NMR results for hexad **6** indicate formation of three similar dimers, which are arranged such that additional electronic interactions occur between the pairs of twist-stacked porphyrins. In triad **3**, interchromophore interactions are present, as indicated by the NMR chemical shift changes relative to **1**, but these interactions are not as strong as they are in **2** and **6**. The zinc series of arrays shows similar behavior, although the chemical shift changes are not as large as they are for the free base series. In principle, this might represent either different twist-stacked conformations in the dimers, or the influence of adjacent dimers. The spectroscopic data discussed below suggest that the second reason is correct.

The molecular modeling performed on **6** is consistent with the NMR results. The chromophores are present as a trimer of dimers (Figure 6). As mentioned above, the calculated conformation does not show the symmetry predicted by the NMR spectra, as all six porphyrins are on one side of the plane of the central benzene ring. However, the calculated structure could be rapidly equilibrating with the same or an enantiomeric structure on the opposite side of the ring plane, and interchange proton environments in the process.

NMR spectroscopy is a relatively slow method, and if intramolecular interconversion of conformations is rapid on the NMR time scale (typically milliseconds or longer), only time-averaged chemical shifts will be observed. For example, the chemical shift change of −3.3 ppm observed for the *meso*-proton of **2** could be due in principle to a single conformation as shown in Figure 5, or an average of a conformation in which the porphyrin macrocycles do not interact to form dimers and one in which the chemical shift change is even greater. Porphyrin ring current models[47] show that the absolute maximum chemical shift change for a proton located at van der Waals separation from a porphyrin is −5.2 ppm, and that this occurs only when the proton is directly over the center of the porphyrin ring. Thus, at the very least, 63% of the dyads would necessarily exist in this dimer conformation. As can be seen from Figure 5, achieving such a conformation would result in significant strain energy in the molecule. Thus, it appears

DOI: 10.1021/ja510267c
J. Am. Chem. Soc. 2015, 137, 245−258

from the NMR data that most or all molecules of **2** (and by extension **6**) in solution exist entirely in twist-stacked dimer conformations. This conclusion is supported by the NOE experiments

This conclusion is also supported by the UV−vis data. Strong $\pi-\pi$ interactions between chromophores can lead to excitonic splittings that are due to electronic interactions of the transition dipoles.[57,58] The absorption spectra of the arrays indicate such excitonic interactions. According to simple exciton theory,[23,57,58] excitonic interactions are determined by the oscillator strengths of the transitions, and the distance and angles between them. Excitonic interactions are often discussed in terms of two extremes. In one of these, the interacting transition dipoles are parallel, and stacked one above the other. In such "face-to-face" arrangements of chromophores (found in intermolecular H-aggregates) transitions to the upper of the two electronic states formed by interaction of the transition dipoles are allowed, resulting in hypsochromic shifts of absorption bands. Once such states are formed, they usually relax rapidly to the lower, forbidden state, and the system shows reduced emission intensities and shortened fluorescence lifetimes. In the other extreme, the transition moments are collinear in a "head-to-tail" arrangement, as observed in intermolecular J-aggregates. The lower-energy excitonic state is the allowed state, which leads to bathochromic shifts in absorption and emission, relatively stronger fluorescence, and reduced excited-state lifetimes. However, these two oft-discussed types of excitonic interaction are only extremes, and many other possibilities exist. In the arrays discussed here, as exemplified by the structure in Figure 5, the transition dipoles are neither coplanar nor collinear. Such conditions can lead to red shifts, blue shifts, no shift, or band splitting in absorption, and small changes in the angles between transition moments can lead to large changes in the nature of the exciton.[23,57,58]

Free base porphyrins have two orthogonal transition moments associated with the B_x and B_y (Soret) band absorptions that pass through the lines connecting opposite *meso*−*meso* positions, and two orthogonal transition moments associated with Q_x and Q_y bands absorption that pass through opposite nitrogen atoms. (The Q_x transition is associated with the protonated nitrogens.) In metalated porphyrins, the two B bands are degenerate, as are the two Q bands, and protonation is impossible. Thus, when two or more porphyrins exhibit excitonic coupling, each transition in one-half of a dimer can couple with two or more transitions in the other, which further complicates excitonic analysis. Excitonic interactions in porphyrin dimers has been observed often, and the subject has been reviewed.[23,73,74]

In the spectrum of dyad **2**, at least two Soret bands are observed, and these are both shifted to shorter wavelengths than the Soret band of monomer **1**. Due to the forbidden nature of the Q transitions, excitonic effects are reduced in this region, and any large shifts of these bands are not observed. However, broadening and small red shifts are seen. These observations are qualitatively consistent with the proposed twist-stacked conformation of **2**, where the molecular planes are roughly parallel, and the two transition moments for each porphyrin are offset from those of the other porphyrin and have different angular relationships to the moments of the other porphyrin. The strong B-bands show blue shifts, which are generally consistent with stacked porphyrins of some type. Given that each porphyrin in a dimer has two B-type transition moments and that each nitrogen will be protonated only part of the time due to rapid exchange of hydrogen atoms, the absorption in these molecules is actually an amalgam of a group of closely related excitonic transitions with different angles between the transition moments. The different angles will lead to different spectral shifts, leading to a broad band, as is observed.[23]

The UV−vis results for **6** are very similar to those for **2**, and this is consistent with the formation of similar dimer-like structures. Three of these will be present in each hexad. Additional interactions between these dimers are also present, as shown especially by additional spectral broadening in the emission spectrum. On the other hand, the excitonic interactions in the absorption spectra are much reduced in triad **3**. This is reasonable, given that the *meta* relationships of the porphyrin linkages at the central benzene ring may restrict the close approach of the chromophores, and that only one dimer may be present at any one time.

The zinc series shows slightly different behavior. In such metalated porphyrins, the two B-type transition moments are degenerate, as are the Q-band transitions. The absorption spectrum of $\mathbf{2Zn_2}$ (Figure 10) shows mainly blue shifts relative to that of **1Zn** due to exciton formation, but also some absorption to longer wavelengths than are found in **1Zn**. Hexad **6Zn** shows similar behavior. Thus, the spectra of these arrays suggest excitonic interactions characteristic of both the blue-shifted (H-type) and red-shifted (J-type) regimes. Addition of pyridine disrupts the excitonic interactions, presumably due to coordination to the zinc atoms to act as fifth ligands.

The fluorescence spectra of the arrays are also consistent with excitonic interactions. The emission spectra of the dyads and free base hexad (Figures 9 and 10) have basically the same shape as that of the monomer, but are quenched. Such quenching is characteristic of cofacial arrangements of porphyrins in which the transition dipoles are stacked.[60,75] In Figure 9 excitation was into the B-bands, which are expected to populate the formally forbidden and short-lived Q-band exciton states, perhaps via the influence of vibronic states,[76] leading to reduced emission intensity. Of special interest is the unusual red shift and loss of vibrational fine structure in the emission spectrum of the zinc hexad **6Zn** (Figure 10b). It is unlikely that this is due to any sort of charge-transfer interaction, as no such behavior was observed in $\mathbf{2Zn_2}$, and Table 2 shows that the two compounds have nearly equal energies for any charge-separated state. It is possible that the red-shifted emission observed for **6Zn** is mainly from more head-to-tail-like arrangements of transition moments with different degrees of bathochromic shift. The situation in the hexads is complex due to the possibility of interaction of transitions in different dimer pairs with one another. The addition of pyridine disrupts the association of the chromophores, resulting in spectra closer to those of porphyrin **1Zn**.

The time-resolved data for all the molecules studied show reduced emission lifetimes, which are consistent with perturbations to the individual porphyrin chromophores due to excitonic interactions. These measurements suggest that several conformations are present for each molecule, and that in all conformations the fluorescence lifetimes are quenched relative to those of **1** or **1Zn**. These lifetimes are those of the Q-band first excited singlet states, which do not show large excitonic interactions in absorption due to their relatively small extinction coefficients, but which in these experiments were populated from the B-states. Shortened fluorescence lifetimes

DOI: 10.1021/ja510267c
J. Am. Chem. Soc. 2015, 137, 245−258

and multiple fluorescence liftetimes have been reported for porphyrin dimers and aggregates of many types, including both H- and J-aggregates.[23,60,74,75,77,78] Typically, the H-aggregates show shorter fluorescence lifetimes than J-aggregates, but both are shorter than those of the monomer. Thus, the results for the arrays studied here are consistent with multiple, structurally closely related conformers, some with more H-aggregate-like character and some with more J-aggregate-like character. This is consistent with twisted stacked conformations similar to those proposed in the dyads and hexads.

Finally, the electrochemical data in Table 2 are also consistent with this general conformational picture. The data for **3** are similar to those for **1**, suggesting relatively little perturbation of the π-systems. For **2** and **6** the potential shifts for the first oxidation, and the reduction in the area of the oxidation wave are consistent with dimer-type interactions in which the radical cation is spread over both porphyrins. A similar situation exists for the zinc series. Negative potential shifts in the first oxidation of porphyrin-like dimers, such as observed with **2** and **6**, have been reported in synthetic[79] and natural[80−82] systems.

METHODOLOGY

Materials. Dichloromethane and toluene were distilled from calcium hydride, and tetrahydrofuran was distilled from sodium/benzophenone under nitrogen. Pyridine (ACS, Mallinckrodt chemicals) and ethanol (200 proof, KOPTEC) were used as purchased. Benzyl bromide (99%, Alfa Aesar), α,α'-dichloro-*o*-xylene (>97%, TCI America), and hexakis(bromomethyl)benzene (TCI America) were used as purchased. The 1,3,5-tris(bromomethyl)benzene was synthesized by a literature method.[83] Sodium bicarbonate (ACS, Mallinckrodt chemicals), potassium hydroxide (technical, JT Baker), zinc acetate dihydrate (Baker analyzed reagent), and tetrabutylammonium fluoride (1 M in THF, Oakwood Products Inc.) were used as purchased. Synthetic procedures for preparation of the previously unknown molecules are presented in the Supporting Information.

General Procedures. All 1D and 2D NMR spectra (gCOSY and NOESY) were recorded on 400 or 500 MHz Varian spectrometers. Selective NOE experiments and analysis to estimate interatomic distances in dyad **2** were performed using published methods.[84] Mass spectra were obtained on an Applied Biosystems Voyager-DE STR matrix-assisted laser desorption/ionization time-of-flight spectrometer (MALDI-TOF). Ultraviolet−visible absorption spectra were measured on a Shimazu UV2100U spectrometer. The solvents for optical and electrochemical measurements were distilled dichloromethane, toluene, or 2-methyltetrahydrofuran as noted. Thin-layer chromatography was performed on silica gel GHFL or GHL (Analtech). Synthesis, TLC, workup, and purification were performed in a darkened laboratory.

Cyclic voltammetry in dichloromethane containing 0.1 M tetra-*n*-butylammonium hexafluorophosphate was performed on a CH Instruments, Inc. potentiostat 420. A glassy carbon electrode was used as the working electrode, and a platinum wire was used as the counter electrode. The reference electrode was a silver wire dipped into 0.01 M silver nitrate in acetonitrile containing 0.1 M tetra-*n*-butylammonium hexafluorophosphate. Ferrocene was added as an internal reference. Cyclic voltammetric data were analyzed by CHI 420B version 11.13 software.

Steady-state fluorescence spectra were measured using a Photon Technology International MP-1 spectrometer and corrected for detection system response as a function of wavelength. Excitation was provided by a 75 W xenon-arc lamp and single-grating monochromator. Fluorescence was detected at 90° to the excitation beam via a single-grating monochromator and an R928 photomultiplier tube having S-20 spectral response and operating in the single photon counting mode. Fluorescence decay measurements were performed on optically dilute (ca. 1×10^{-5} M) samples by the time-correlated single-photon-counting method. Two different excitation systems were employed. The excitation source for the first system was a mode-locked Ti:sapphire laser (Spectra Physics, Millennia-pumped Tsunami) with a 130 fs pulse duration operating at 80 MHz. The laser output was sent through a frequency doubler and pulse selector (Spectra Physics model 3980) to obtain 370−450 nm pulses at 4 MHz. The excitation source for the second system was a fiber supercontinuum laser based on a passive modelocked fiber laser and a high-non-linearity photonic crystal fiber supercontinuum generator (Fianium SC450). The laser provides 6 ps pulses at a repetition rate variable between 0.1 and 40 MHz. The laser output was sent through an Acousto-Optical Tunable Filter (Fianium AOTF) and the relevant 10 nm interference filter to obtain excitation pulses at a desired wavelength. Fluorescence emission was detected at the magic angle using a double-grating monochromator (Jobin Yvon Gemini-180) and a microchannel plate photomultiplier tube (Hamamatsu R3809U-50). The instrument response function was 35−65 ps. The spectrometer was controlled by software based on the LabView programming language, and data acquisition was done using a single photon counting card (Becker-Hickl, SPC-830). Fluorescence anisotropy decays were obtained by changing the detection polarization of the fluorescence path parallel or perpendicular to the polarization of the excitation light. The anisotropy decays then were calculated according to eq 1, where $I_{VV}(t)$ (or $I_{VH}(t)$) is the fluorescence decay when the

$$r(t) = \frac{I_{VV}(t) - GI_{VH}(t)}{I_{VV}(t) + 2GI_{VH}(t)} \quad (1)$$

excitation light is vertically polarized and only the vertically (or horizontally) polarized portion of fluorescence is detected, denoting that the first and second subscripts represent excitation and detection polarization, respectively. The factor G, which is equal to the ratio of the sensitivities of the detection system for vertically and horizontally polarized light, can be determined either by so-called tail matching of $I_{VV}(t)$ and $I_{VH}(t)$ or by $I_{HV}(t)/I_{HH}(t)$.

Data analysis was carried out using locally written software (ASUFIT) developed under a MATLAB environment (Mathworks Inc.). Random errors associated with the reported lifetimes obtained from fluorescence measurements were typically ≤5%.

Quantum Chemical Modeling. The structure of hexad **6**, was modeled using a dispersion-corrected DFT B3LYP/6-31+G(d,p) method with corrections implemented using carbon atom-centered effective core-type potentials.[53,85] Dispersion corrected potentials were generated using DCPgen v1.9 software obtained from DiLabio's research group at the University of Alberta (www.ualberta.ca/~gdilabio). The structure optimizations were performed using the Gaussian 09 software package on a 48-core PC cluster. The SCF convergence criterion was relaxed to the 10-5 level to facilitate convergence within a reasonable time. No orbital symmetry constraints were imposed.

CONCLUSIONS

The new porphyrin preparation method that we have reported earlier has allowed facile synthesis of a series of porphyrin arrays in which the macrocycles are distributed around a central benzene ring. The nature of the chemical linkage to this central ring allows the π-systems of the porphyrins to approach one another closely, and this in turn leads to strong interchromophore interactions showing excitonic splitting of transitions. Dyad **2** assumes conformations in which the two macrocycles are arranged in a twist-stacked geometry with C_2 symmetry. Approximately half of each porphyrin ring is stacked with the corresponding half of the other porphyrin with an essentially van der Waals separation. Hexad **6** exists as a trimer of similar dimers, and all of the porphyrins interact electronically to some extent. The triad **3** shows much weaker interactions among the three porphyrins, perhaps including transient conformations in

DOI: 10.1021/ja510267c
J. Am. Chem. Soc. 2015, 137, 245−258

which two porphyrins form dimers and the third is relatively far from the other two. The zinc series of molecules shows similar behavior, and the interactions between chromophores are strongly reduced by addition of pyridine, which coordinates to the zinc atoms.

The UV−vis spectra indicate excitonic splitting in the dimers in the various molecules. These interactions are generally of the type in which the upper excitonic level is more allowed, resulting in absorption shifts to shorter wavelengths. However, the exact nature of the interactions depends in detail upon the interchromophore separations and the relative orientations of the transition dipoles in each conformation.

Singlet−singlet energy transfer is observed in $\mathbf{2Zn_1}$, where the chromophores are different, with a rate constant of ca. 2.3×10^{10} s^{-1}. Anisotropy studies of the other arrays show that energy transfer among identical chromophores occurs with time constants on the order of 150 ps or less.

The more facile oxidation of the arrays that feature dimer formation and the suggested sharing of the radical cation between the two macrocycles in the dimer are both characteristic of the special pair of bacteriochlorophylls in some bacterial photosynthetic reaction centers. Thus, **2** and $\mathbf{2Zn_2}$ are potentially good models for some aspects of the properties of these reaction centers.

Finally, strongly interacting chlorophyll molecules in photosynthetic antenna systems sometimes show quantum coherence effects upon light absorption, and this may play a role in the rapid energy transfer between such chromophores. It would be interesting to investigate any such effects in these arrays or similar ones.

■ ASSOCIATED CONTENT

Ⓢ Supporting Information

Synthesis and characterization of the compounds reported, temperature-dependent NMR spectra, fluorescence anisotropy decays, cyclic voltammograms, and chemical shift change calculations based on porphyrin ring currents. This material is available free of charge via the Internet at http://pubs.acs.org.

■ AUTHOR INFORMATION

Corresponding Authors

amoore@asu.edu
tmoore@asu.edu
gust@asu.edu

Notes

The authors declare no competing financial interest.

■ ACKNOWLEDGMENTS

This work was supported by the Office of Basic Energy Sciences, Division of Chemical Sciences, Geosciences, and Energy Biosciences, U.S. Department of Energy under contract DE-FG02-03ER15393 and the Center for Bio-Inspired Solar Fuel Production, an Energy Frontier Research Center funded by the U.S. Department of Energy, Office of Science, Office of Basic Energy Sciences under Award No. DE-SC0001016.

■ REFERENCES

(1) Blankenship, R. E.; Madigan, M. T.; Bauer, C. E. *Anoxygenic Photosynthetic Bacteria*, 1st ed.; Kluwer: Dordrecht, 1995; Vol. 2.
(2) Knaff, D. B. *Photosynth. Res.* **2005**, *83*, 99−100.
(3) Orf, G. S.; Blankenship, R. E. *Photosynth. Res.* **2013**, *116*, 315−331.
(4) Chen, M.; Scheer, H. *J. Porphyrins Phthalocyanines* **2013**, *17*, 1−15.
(5) McDermott, G.; Prince, S. M.; Freer, A. A.; Hawthornthwaite-Lawless, A. M.; Papiz, M. Z.; Cogdell, R. J.; Isaacs, N. W. *Nature* **1995**, *374*, 517−521.
(6) Deisenhofer, J.; Epp, O.; Miki, K.; Huber, R.; Michel, H. *Nature* **1985**, *318*, 618−624.
(7) Deisenhofer, J.; Michel, H. *Science* **1989**, *245*, 1463−1473.
(8) O'Sullivan, M. C.; Sprafke, J. K.; Kondratuk, D. V.; Rinfray, C.; Claridge, T. D.; Saywell, A.; Blunt, M. O.; O'Shea, J. N.; Beton, P. H.; Malfois, M.; Anderson, H. L. *Nature* **2011**, *469*, 72−75.
(9) Hori, T.; Aratani, N.; Takagi, A.; Matsumoto, T.; Kawai, T.; Yoon, M. C.; Yoon, Z. S.; Cho, S.; Kim, D.; Osuka, A. *Chem.—Eur. J.* **2006**, *12*, 1319−1327.
(10) Cho, S.; Li, W. S.; Yoon, M. C.; Ahn, T. K.; Jiang, D. L.; Kim, J.; Aida, T.; Kim, D. *Chem.—Eur. J.* **2006**, *12*, 7576−7584.
(11) Morandeira, A.; Vauthey, E.; Schuwey, A.; Gossauer, A. *J. Phys. Chem. A* **2004**, *108*, 5741−5751.
(12) Peng, X. B.; Aratani, N.; Takagi, A.; Matsumoto, T.; Kawai, T.; Hwang, I. W.; Ahn, T. K.; Kim, D.; Osuka, A. *J. Am. Chem. Soc.* **2004**, *126*, 4468−4469.
(13) Khoury, R. G.; Jaquinod, L.; Aoyagi, K.; Olmstead, M. M.; Fisher, A. J.; Smith, K. M. *Angew. Chem., Int. Ed.* **1997**, *36*, 2497−2500.
(14) Hao, E. H.; Fronczek, F. R.; Vicente, M. G. H. *J. Org. Chem.* **2006**, *71*, 1233−1236.
(15) Davila, J.; Harriman, A.; Milgrom, L. R. *Chem. Phys. Lett.* **1987**, *136*, 427−430.
(16) Jiang, H. W.; Ham, S.; Aratani, N.; Kim, D.; Osuka, A. *Chem.—Eur. J.* **2013**, *19*, 13328−13336.
(17) Li, J. Z.; Ambroise, A.; Yang, S. I.; Diers, J. R.; Seth, J.; Wack, C. R.; Bocian, D. F.; Holten, D.; Lindsey, J. S. *J. Am. Chem. Soc.* **1999**, *121*, 8927−8940.
(18) Li, J. Z.; Diers, J. R.; Seth, J.; Yang, S. I.; Bocian, D. F.; Holten, D.; Lindsey, J. S. *J. Org. Chem.* **1999**, *64*, 9090−9100.
(19) Li, J. Z.; Lindsey, J. S. *J. Org. Chem.* **1999**, *64*, 9101−9108.
(20) Ogawa, K.; Kobuke, Y. *Angew. Chem., Int. Ed.* **2000**, *39*, 4070−4073.
(21) Parkinson, P.; Knappke, C. E. I.; Kamonsutthipaijit, N.; Sirithip, K.; Matichak, J. D.; Anderson, H. L.; Herz, L. M. *J. Am. Chem. Soc.* **2014**, *136*, 8217−8220.
(22) Satake, A.; Azuma, S.; Kuramochi, Y.; Hirota, S.; Kobuke, Y. *Chem.—Eur. J.* **2011**, *17*, 855−865.
(23) Satake, A.; Kobuke, Y. *Org. Biomol. Chem.* **2007**, *5*, 1679−1691.
(24) Hwang, I. W.; Park, M.; Ahn, T. K.; Yoon, Z. S.; Ko, D. M.; Kim, D.; Ito, F.; Ishibashi, Y.; Khan, S. R.; Nagasawa, Y.; Miyasaka, H.; Keda, C.; Takahashi, R.; Ogawa, K.; Satake, A.; Kobuke, Y. *Chem.—Eur. J.* **2005**, *11*, 3753−3761.
(25) Khoury, R. G.; Jaquinod, L.; Aoyagi, K.; Olmstead, M. M.; Fisher, A. J.; Smith, K. M. *Angew. Chem., Int. Ed.* **1997**, *36*, 2497−2500.
(26) Kodis, G.; Terazono, Y.; Liddell, P. A.; Andréasson, J.; Garg, V.; Hambourger, M.; Moore, T. A.; Moore, A. L.; Gust, D. *J. Am. Chem. Soc.* **2006**, *128*, 1818−1827.
(27) Terazono, Y.; Kodis, G.; Liddell, P. A.; Garg, V.; Moore, T. A.; Moore, A. L.; Gust, D. *J. Phys. Chem. B* **2009**, *113*, 7147−7155.
(28) Terazono, Y.; Kodis, G.; Bhushan, K.; Zaks, J.; Madden, C.; Moore, A. L.; Moore, T. A.; Fleming, G. R.; Gust, D. *J. Am. Chem. Soc.* **2011**, *133*, 2916−2922.
(29) Garg, V.; Kodis, G.; Liddell, P. A.; Terazono, Y.; Moore, T. A.; Moore, A. L.; Gust, D. *J. Phys. Chem. B* **2013**, *117*, 11299−11308.
(30) Cho, H. S.; Rhee, H.; Song, J. K.; Min, C.-K.; Takase, M.; Aratani, N.; Cho, S.; Osuka, A.; Joo, T.; Kim, D. *J. Am. Chem. Soc.* **2003**, *125*, 5849−5860.
(31) Garg, V.; Kodis, G.; Chachisvilis, M.; Hambourger, M.; Moore, A. L.; Moore, T. A.; Gust, D. *J. Am. Chem. Soc.* **2011**, *133*, 2944−2954.
(32) Liddell, P. A.; Kodis, G.; de la Garza, L.; Moore, A. L.; Moore, T. A.; Gust, D. *J. Phys. Chem. B* **2004**, *108*, 10256−10265.
(33) Terazono, Y.; Liddell, P. A.; Garg, V.; Kodis, G.; Brune, A.; Hambourger, M.; Moore, T. A.; Moore, A. L.; Gust, D. *J. Porphyrins Phthalocyanines* **2005**, *9*, 706−723.

DOI: 10.1021/ja510267c
J. Am. Chem. Soc. 2015, 137, 245−258

(34) Hoyer, S.; Ishizaki, A.; Whaley, K. *Phys. Rev. E* **2012**, *86*, No. 041911.
(35) Engel, G. S.; Calhoun, T. R.; Read, E. L.; Ahn, T. K.; Mancal, T.; Cheng, Y. C.; Blankenship, R. E.; Fleming, G. R. *Nature* **2007**, *446*, 782−786.
(36) Ishizaki, A.; Fleming, G. R. *Proc. Natl. Acad. Sci. U.S.A.* **2009**, *106*, 17255−17260.
(37) Lee, H.; Cheng, Y. C.; Fleming, G. R. *Science* **2007**, *316*, 1462−1465.
(38) Schlau-Cohen, G. S.; Ishizaki, A.; Calhoun, T. R.; Ginsberg, N. S.; Ballottari, M.; Bassi, R.; Fleming, G. R. *Nat. Chem.* **2012**, *4*, 389−395.
(39) Collini, E.; Wong, C. Y.; Wilk, K. E.; Curmi, P. M. G.; Brumer, P.; Scholes, G. D. *Nature* **2010**, *463*, 644−647.
(40) Scholes, G. D. *J. Phys. Chem. Lett.* **2010**, *1*, 2−8.
(41) Fleming, G. R.; van Grondelle, R. *Curr. Opin. Struct. Biol.* **1997**, *7*, 738−748.
(42) van Grondelle, R.; Novoderezhkin, V. I. *Nature* **2010**, *463*, 614−615.
(43) Terazono, Y.; North, E. J.; Moore, A. L.; Moore, T. A.; Gust, D. *Org. Lett.* **2012**, *14*, 1776−1779.
(44) Wu, C. Y.; Brik, A.; Wang, S. K.; Chen, Y. H.; Wong, C. H. *ChemBioChem* **2005**, *6*, 2176−2180.
(45) Biemans, H. A. M.; Rowan, A. E.; Verhoeven, A.; Vanoppen, P.; Latterini, L.; Foekema, J.; Schenning, A. P. H. J.; Meijer, E. W.; de Schryver, F. C.; Nolte, R. J. M. *J. Am. Chem. Soc.* **1998**, *120*, 11054−11060.
(46) Rao, P. D.; Dhanalekshmi, S.; Littler, B. J.; Lindsey, J. S. *J. Org. Chem.* **2000**, *65*, 7323−7344.
(47) Cross, K. J.; Crossley, M. J. *Aust. J. Chem.* **1992**, *45*, 991−1004.
(48) Deisenhofer, J.; Epp, O.; Sinning, I.; Michel, H. *J. Mol. Biol.* **1995**, *246*, 429−457.
(49) Abraham, R. J.; Hawkes, G. E.; Smith, K. M. *Tetrahedron Lett.* **1974**, 1483−1486.
(50) Eaton, S. S.; Eaton, G. R. *J. Am. Chem. Soc.* **1977**, *99*, 1601−1604.
(51) Storm, C. B.; Teklu, Y. *J. Am. Chem. Soc.* **1972**, *94*, 1745-&.
(52) Storm, C. B.; Teklu, Y.; Sokolosk.Ea. *Ann. N.Y. Acad. Sci.* **1973**, *206*, 631−640.
(53) Torres, E.; DiLabio, G. A. *J. Phys. Chem. C* **2012**, *3*, 1738−1744.
(54) Lill, S. O. *Phys. Chem. Chem. Phys.* **2011**, *13*, 16022−16027.
(55) Eisner, U.; Linstead, R. P. *J. Chem. Soc.* **1955**, 3749−3754.
(56) Barnett, G. H.; Hudson, M. F.; Smith, K. M. *J. Chem. Soc., Perkin Trans. 1* **1975**, 1401−1403.
(57) Kasha, M.; Rawls, H. R.; Ashraf El-Bayoumi, A. *Pure Appl. Chem.* **1965**, *11*, 371−392.
(58) McRae, E. G.; Kasha, M. *Physical Processes in Radiation Biology*; Academic Press: New York, 1964.
(59) Kasha, M.; Elbayoumi, M. A.; Rhodes, W. *J. Chim. Phys. Phys.-Chim. Bio.* **1961**, *58*, 916−925.
(60) Verma, S.; Ghosh, A.; Das, A.; Ghosh, H. N. *J. Phys. Chem. B* **2010**, *114*, 8327−8334.
(61) Verma, S.; Ghosh, H. N. *J. Phys. Chem. C* **2012**, *3*, 1877−1884.
(62) Ojadi, E.; Selzer, R.; Linschitz, H. *J. Am. Chem. Soc.* **1985**, *107*, 7783−7784.
(63) Ribo, J. M.; Bofill, J. M.; Crusats, J.; Rubires, R. *Chem.—Eur. J.* **2001**, *7*, 2733−2737.
(64) Arai, Y.; Segawa, H. *J. Phys. Chem. B* **2011**, *115*, 7773−7780.
(65) Guo, L. *J. Colloid Interface Sci.* **2008**, *322*, 281−286.
(66) Monteiro, C. J.; Pereira, M. M.; Vicente, M.; Arnaut, L. G. *Tetrahedron* **2012**, *68*, 8783−8788.
(67) Sen, A.; Krishnan, V. *J. Chem. Soc., Faraday Trans.* **1997**, *93*, 4281−4288.
(68) Schmitz, R. A.; Liddell, P. A.; Kodis, G.; Kenney, M. J.; Brennan, B. J.; Oster, N. V.; Moore, T. A.; Moore, A. L.; Gust, D. *Phys. Chem. Chem. Phys.* **2014**, *16*, 17569−17579.
(69) Förster, T. *Ann. Phys.* **1948**, *2*, 55−75.
(70) Förster, T. *Discuss. Faraday Soc.* **1959**, *27*, 7−17.
(71) Connelly, N. G.; Geiger, W. E. *Chem. Rev.* **1996**, *96*, 877−910.
(72) Norris, J. R.; Uphaus, R. A.; Crespi, H. L.; Katz, J. *Proc. Natl. Acad. Sci. U.S.A.* **1971**, *68*, 625−628.
(73) Harvey, P. D.; Stern, C.; Gros, C. P.; Guilard, R. *Coord. Chem. Rev.* **2007**, *251*, 401−428.
(74) Andrade, S. M.; Teixeira, R.; Costa, S. M.; Sobral, A. J. *Biophys. Chem.* **2008**, *133*, 1−10.
(75) Chang, C. J.; Baker, E. A.; Pistorio, B. J.; Deng, Y. Q.; Loh, Z. H.; Miller, S. E.; Carpenter, S. D.; Nocera, D. G. *Inorg. Chem.* **2002**, *41*, 3102−3109.
(76) Akins, D. L.; Ozcelik, S.; Zhu, H. R.; Guo, C. *J. Phys. Chem.* **1996**, *100*, 14390−14396.
(77) Misawa, K.; Kobayashi, T. *J. Chem. Phys.* **1999**, *110*, 5844−5850.
(78) Ozcelik, S.; Akins, D. L. *J. Phys. Chem. B* **1999**, *103*, 8926−8929.
(79) Takai, A.; Gros, C. P.; Barbe, J. M.; Guilard, R.; Fukuzumi, S. *Chem.—Eur. J.* **2009**, *15*, 3110−3122.
(80) Davis, M. S.; Forman, A.; Hanson, L. K.; Thornber, J. P.; Fajer, J. *J. Phys. Chem.* **1979**, *83*, 3325−3332.
(81) Breton, J.; Xu, W.; Diner, B. A.; Chitnis, P. R. *Biochemistry* **2002**, *41*, 11200−11210.
(82) Kanchanawong, P.; Dahlbom, M. G.; Treynor, T. P.; Reimers, J. R.; Hush, N. S.; Boxer, S. G. *J. Phys. Chem. B* **2006**, *110*, 18688−18702.
(83) Wang, L.; Yi, W. b.; Cai, C. *Chem. Commun.* **2011**, *47*, 806−808.
(84) Butts, C. P.; Jones, C. R.; Towers, E. C.; Flynn, J. L.; Appleby, L.; Barron, N. J. *Org. Biomol. Chem.* **2011**, *9*, 177−184.
(85) Mackie, I. D.; DiLabio, G. A. *J. Phys. Chem. A* **2008**, *112*, 10968−10976.

DOI: 10.1021/ja510267c
J. Am. Chem. Soc. 2015, 137, 245−258